A&A 372, 676–685 (2001)
DOI: 10.1051/0004-6361:20010379

Astronomy & Astrophysics

Moreton wave and its source of disturbances in the X12/3B WLF of AR6659 in 1991 June 4

H. Zhang⋆

Yunnan Observatory, Chinese Academy of Sciences, Kunming, 650011, PR China
National Astronomical Observatories, Chinese Academy of Sciences, Beijing, 100012, PR China

Received 17 November 1998 / Accepted 14 March 2001

Abstract. The Moreton wave that accompanied the X12/3B June 4 1991 white light flare (WLF) is analyzed. The wave, with a wavelength of 1.4×10^4 km, propagated along the solar limb on the chromosphere, and the wavefronts were accelerated during the propagation: their velocity increased from 2500 $\mathrm{km\,s^{-1}}$ to 4000 $\mathrm{km\,s^{-1}}$. The analyses show that the wave originated in the layers of the atmosphere between the photosphere and the upper chromosphere, and it is suggested that both a magneto-hydrodynamic (MHD) disturbance and a gas-dynamic disturbance are coupled to induce the wave. The MHD disturbance is caused by a rapid variation of the magnetic field, which merges and alternatively emerges. A gas-dynamic disturbance is produced by a strong downward compression of the deep chromosphere and a spray upward ejection occurring simultaneously in the disturbance source region. In the disturbance source, the increase in the magnetic pressure is responsible for the wave acceleration. The photospheric (longitudinal) magnetic field of the source emerges continually during the wavefront propagation, and the corresponding magnetic pressure also increases. The wavefronts that are carried by the plasma around the disturbance source are accelerated, since the transverse pressure compresses the plasma. The observed results do not support the hypothesis that the Moreton wave is the "sweeping skirt" of the shock wavefront, as proposed by Uchida (1974).

Key words. Sun: flares – Sun: magnetic fields – Sun: chromosphere

1. Introduction

A Moreton wave is a flare-associated phenomenon, first observed by Moreton (1963) as a propagating chromospheric disturbance that accompanied a flare. According to the report of Smith & Harvey (1971), the wave is observed in Hα or in H$\alpha \pm 0.5$ Å; its mean chromospheric velocities are in the range of 440 $\mathrm{km\,s^{-1}}$–1125 $\mathrm{km\,s^{-1}}$. The wavefronts present as a dark leading edge and a bright wake in H$\alpha + 0.5$ Å, or as a bright leading edge and a dark wake in the H$\alpha - 0.5$ Å (Dodson & Hedeman 1968). These may result from the depression and relaxation of chromospheric structures. The bright emission fronts are produced by material ejecta seen projected on the disk (Smith & Harvey 1971). In the majority of cases (70%), the angular width of the observed wavefronts is less than 90°, and in the rest of the cases (30%), the angular width is more than 100°. The flare-associated wave is well associated with Type II bursts (e.g. Wild 1968). Sprays were associated with flare waves in the case of the flare on August 28, 1968. Zirin & Russo Lackner (1969) identified the origin of the wave as a spray. Relating Moreton waves with sprays, and with Type II bursts, appears very attractive, since the similarity in velocity of these phenomena suggests that they may be different aspects of the same basic process. Recent EIT observations (Moses et al. 1997) showed a coronal mass ejection (CME), tentatively identified as a coronal manifestation of a "Moreton wave".

A Moreton wave is regarded as the propagation of a MHD disturbance produced in a flare. However, the properties of the disturbance source are far from being established, because identification of both its precise location and time of onset is difficult. The most active region during the 22 solar maximum, NOAA AR6659, (e.g. Zhang Hongqi et al. 1994; Zhang Heng et al. 1996) produced a white light flare X12/3B (beginning at 03:37:25 UT and maximum at 03:39 UT) on June 4 1991. A Moreton wave, a spray and Type II bursts accompanied the flare (Sakurai et al. 1995). The wave moved towards the North Pole along the solar limb, and the distance of propagation was 1.4 times the solar radius on a time scale of about 270 s. The velocity of the wavefronts was initially about 2500 $\mathrm{km\,s^{-1}}$ and later it reached 4000 $\mathrm{km\,s^{-1}}$ when the wavefronts approached to the North Pole (Sakurai et al. 1995). In other words, the fronts were obviously accelerated. The maximum velocity of 4000 $\mathrm{km\,s^{-1}}$ of the wave after acceleration is probably the largest ever observed.

The flare was observed with the Magnetic Field Telescope (MFT) of the Beijing Astronomical Observatory (BAO) in Huairou, Beijing, China, and the magnetic fields, velocity fields and monochromatic images at two

⋆ e-mail: hngzhang@public.km.yn.cn

wavelengths (i.e. Hβ:λ4681 Å in the chromosphere and λ5324 Å in the photosphere) were recorded. The flare process was also videotaped by both the Solar Flare Telescope (SFT) and the Hα full disk flare patrol telescope of the National Astronomical Observatory of Japan (NAOJ, Mitaka). The data recorded by the SFT are the chromospheric Hα intensity within a FOV of $5' \times 5'$. The Moreton wave is quite obviously displayed on the videotape obtained with the flare patrol telescope. Fortunately, the MFT of BAO recorded the Hβ intensity and velocity field map of the Moreton wave when its wavefronts were still within the view-field of the telescope. These data are quite precious for us to study the relationship of the wave to the accompanying spray, especially in order to study the origin and the wavefronts of the Moreton wave.

2. Observations of the wavefronts and origin of the Moreton wave

2.1. Spray and wavefronts

2.1.1. Spray and its origin

Figure 1 shows the Hβ image of the flare observed with the MFT. During the maximum of the flare, the two bright ribbons, which can be seen in the left-bottom quadrant of the figure, covered the umbra of the major sunspot and were positioned in two areas with opposite polarities. The two ribbons separated gradually after the maximum, while the post-flare loops (with the ribbons as their "foot points") gradually ascended (Zhang Hongqi et al. 1994). This was a typical two-ribbon flare. We regard the two bright ribbons as the main part of the flare (cf. Fig. 3d). In the region to the north (right-upper quadrant of Fig. 1) of the main flare, there is an arc-shaped emission belt. This emission belt is the projection of a spray against the disk. The spray ejecting process can be seen clearly in the Hα video recording, and its formation process is schematically shown in frames of Fig. 2. At 03:38:52 UT the "origin of spray" (i.e. the brightest kernels in the small rectangle of Fig. 1) starts to brighten (Fig. 2a). Then the spray material was ejected about 3 degrees toward the east (Fig. 2b), which means that the material moved upward with a velocity of 617 km s^{-1}, because the active region AR6659, which was the origin of the spray material, was located at N30°E70° on the solar disk. Afterwards, the front-tip (marked "front-tip" in Fig. 2) of the spray material moved 30 000 km along the solar surface in 3 s from 03:38:58 UT to 03:39:01 UT (Figs. 2b,c). Therefore, the velocity of the spray may be estimated as 10 000 km s^{-1}. This velocity is probably the largest velocity ever reported on the chromosphere. In addition, the rapidly developing processes can be seen in the Hα video recording, and are schematically shown in Figs. 2d–i. First, the brightness at the most curved portion (the "brightness increasing" in Fig. 2d) of the arc-shaped emission trace increased. Second, almost at the same time, a section of bright matter (marked with "matter escaping") "escaped" from the trace where the spray passed through (Figs. 2e,f). Finally, the Moreton wavefront (dotted-dashed line in Fig. 2g), initiated near the south of the trace, began to expand across the trace (Fig. 2h), and propagated toward the solar North Pole from the north of the "matter escaping" region (Fig. 2i). The spray region disappeared from the disk at 03:41:54 UT (Figs. 2i, 3c), after only 3 min.

2.1.2. Wavefronts seen on the chromosphere

The wavefront of the Moreton wave can be seen in the field of view of SFT (Fig. 3a,b) and MFT (Fig. 3c). In Figs. 3a and 3b the wavefront is clearly visible and in Fig. 3c it can be seen faintly, with a brightness lower than that of the plages in other active regions on the solar disk. The shape of the wavefront is similar to the arc-shaped trace of the spray (Fig. 1). The wavefront seems to become the "south (Fig. 2g) and north envelopes" (Figs. 2h,i) of both sides of the spray trace, and the origin of the spray is located in the geometric center of the arc-like wavefront (Fig. 3d). During the propagation of the Moreton wave (i.e. in 270 s from 03:39:34UT to 03:44:04UT), the wavefront basically kept this shape and moved toward the North Pole. Although the similarity of the wavefront with the spray trace is obvious, the spray cannot be identified as the origin of the wave, because the wavefront was seen as sweeping across the spray trace (Fig. 2g) but was not seen as "originating from" the spray.

2.1.3. Position of the wave fronts in the chromospheric velocity field

A chromospheric (Hβ, λ4861 Å) velocity field map was recorded by MFT at BAO. Figure 4 shows the Hβ velocity field as a map in gray scale of AR6659 in June 4, 1991. The line-of-sight velocity was integrated over the time interval 03:39:18.9-03:39:24UT. Two arc-shaped black belts (red shift) and white belts (blue shift) can be seen in the figure. Four dotted lines, overlapped on the map, outline the location and extension of these belts ("$t1$" and "$t2$" outline the black belts, "$c1$" and "$c2$' outline the white-belts). The 4 dotted lines in Fig. 4 are arranged in 4 concentric circles. The dotted line "$c2$" was also drawn on the corresponding location in Fig. 1, in order to identify its counterpart on the chromosphere. Figure 1 shows that "$c2$" is shaped like the spray trace (Fig. 1), and extends north of it. By comparison, Figs. 3a–c show that the wavefronts are also shaped like the spray trace, and also extend north of it. Therefore, the white belt outlined by "$c2$" follows the wavefront-track. The velocity field with this pattern of 4 concentric circles (Fig. 4) suggests that this is the velocity structure of "traveling waves". The arc circles are the tracks left by the traveling waves: the red shift (depression) belts are track of troughs while the blue shift (relaxation) are track of crests, which are perpendicular to the direction of the Moreton wave propagation.

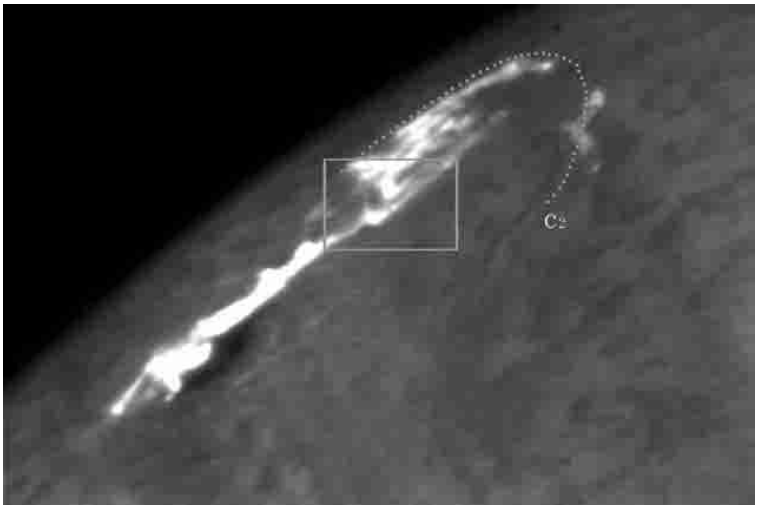

Fig. 1. The chromospheric Hβ intensity field of AR6659 at 03:39:01UT June 4, 1991. The dotted line is same as that shown by "$c2$" in Fig. 4 (see the text). The brightest patches in the rectangle are the origin of the spray. North is up, and east is left.

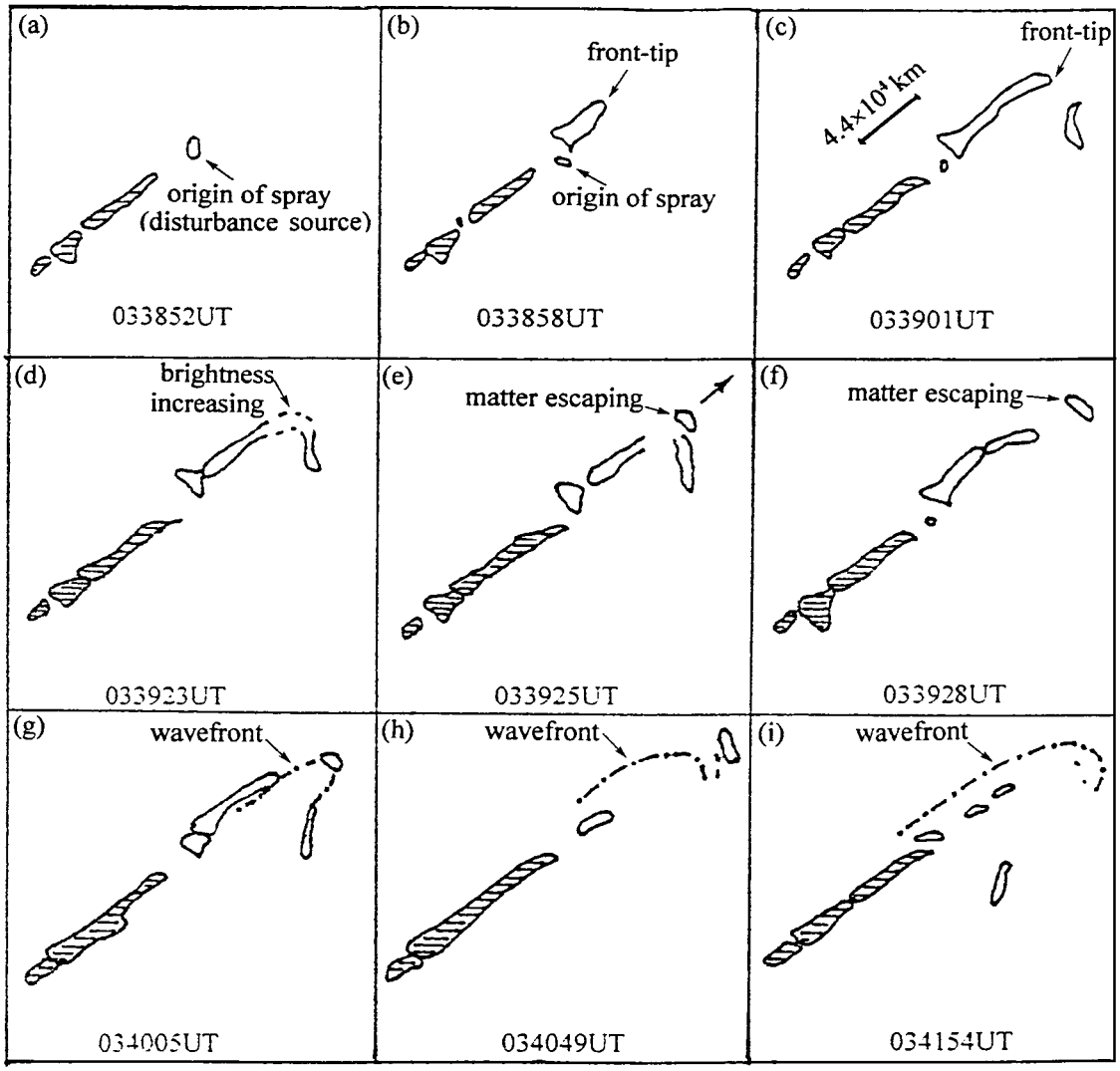

Fig. 2. Schematic sketches showing the rapid development of the spray seen in Fig. 1, based on the Hα video recording (NAOJ, Mitaka) and on the Hβ image (BAO, Huairou). The hatched areas correspond to the main parts (ribbons) of the flare.

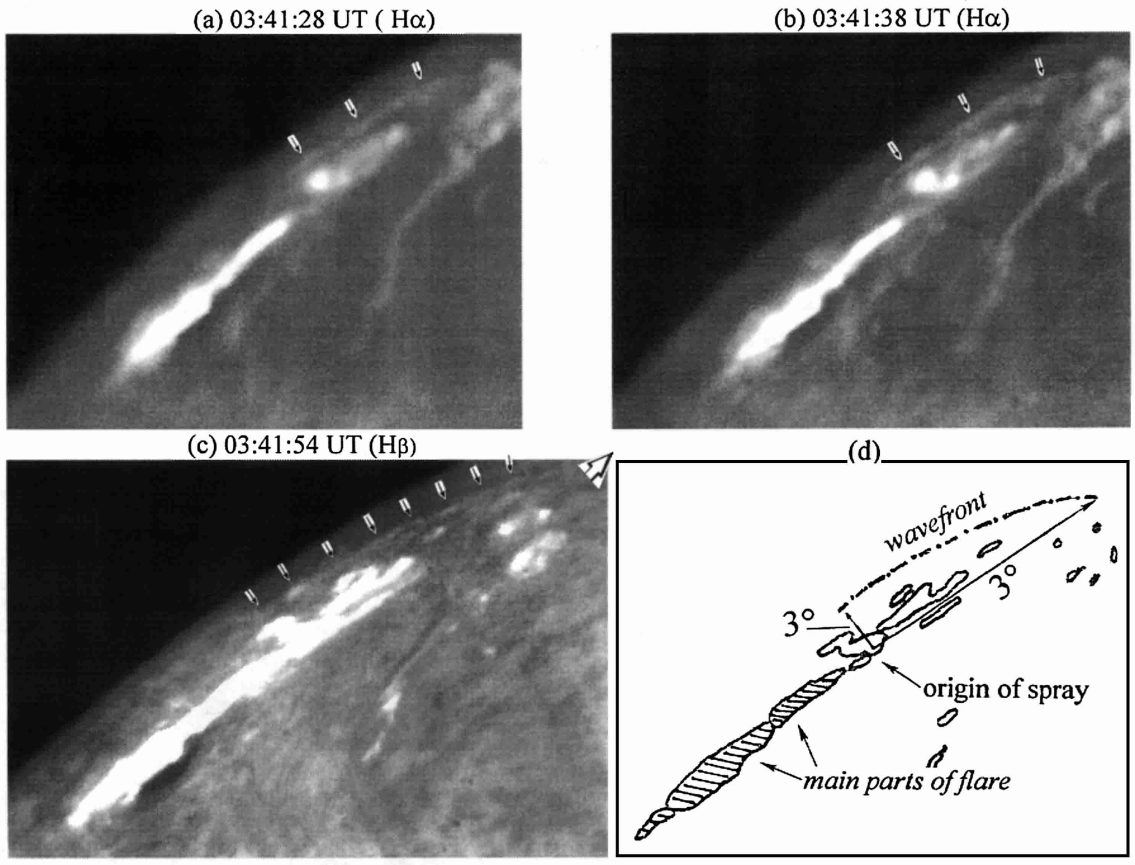

Fig. 3. a),b) The chromospheric Hα intensity field of AR6659, arrows show the wavefronts, and the empty arrow indicates their propagation direction (along the solar limb toward the North Pole). **c)** same as the previous but in Hβ intensity. **d)** Schematic sketch showing the wavefronts and their geometric center ("origin of the spray") (Fig. 2), which is at a distance of 3 spherical degrees from the wavefronts. The hatched areas are the same as in Fig. 2.

In other words, the two troughs ("$t1$" and "$t2$") and the two crests ("$c1$" and "$c2$") were recorded in the velocity field (Fig. 4), although there are no counterparts on the chromosphere which are coincident with the location of the first crest ("c1"). The distance between the two crests is roughly equal to the distance between the two troughs, giving a wavelength equal to 1.4×10^4 km.

2.2. The source of the Moreton wave

2.2.1. Identification of the source of the Moreton wave

The location of the small rectangle in the velocity map Fig. 4 is same as the one in Fig. 1. Within this region, there is a very prominent red-shift area, which is not only at the geometric center of the 4 concentric circles (i.e. wavefronts), but corresponds to the origin of the spray seen on the chromosphere (Fig. 1). Therefore, the red-shift area is the center of the wavefronts, i.e. the source of the Moreton wave. In other words, the spray and the wave originate in the same source, and the wavefronts are shaped like the spray trace, as mentioned above. Thus, while the spray is observed in the chromospheric Hα (Fig. 2) and Hβ (Fig. 1) brightness field, not only the crests and troughs, but also the source of the disturbance are present in the velocity field recording. The distance from the source to the second crest (marked by "c_2") is 7.5×10^4 km, and to the first crest (marked by "c_1") is 8.9×10^4 km, giving a wavelength of 1.4×10^4 km (cf. Sect. 2.1.3).

2.2.2. The vortex-like velocity field

Figure 5 is a magnified map of the velocity field within the rectangle of Fig. 4, i.e. the velocity field of the source. We see from Fig. 5 that the redshift areas of the source have a non-uniform distribution of the velocity field with "fine structures". In the map, the darkest places are thread-like and show greater red line-of-sight velocity at the places outlined by three dashed lines, with a lower relative velocity in the spaces between the threads. The width of the thread is about $4.2''$, with the spacing (where the velocity is lower) being about $5''$ (no correction for projection is made). In addition, the middle thread (or the middle dashed line) is twisted: its center segment goes roughly along the E-W direction, but its western and eastern ends curve toward the north and south, respectively. The pattern constructed by the threads (the red-shift Doppler velocity) reminds one of a cross-section of a downward vortex-like plasma bubble, the morphology of which suggests a strong compression on the deep chromosphere,

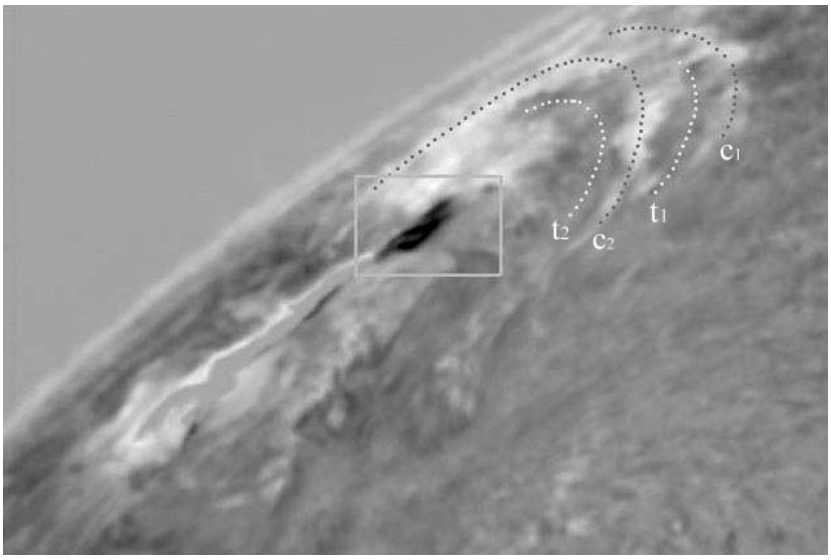

Fig. 4. Gray-scaled Hβ velocity map of AR6659 at 03:39:24UT, the black represents redshift Doppler velocity, and the white represents blueshift. The four dotted lines outline the location and extension, respectively, for two redshift belts shown by "$t1$" and "$t2$", and for two blueshift belts, shown by "$c1$" and "$c2$". The location of the small rectangle is same as in Fig. 1.

Fig. 5. The velocity field map of the area within the small rectangle (disturbance source of the Moreton wave) in Fig. 4. Three dashed lines extend along the places where the line-of-sight velocity is greater in the source.

probably resulting from hot vortical material expanding violently in the upper chromosphere (Fang 1997). The vortex-like velocity field of the disturbance source is relaxed at 03:45:05 UT, where more mechanical energy is released.

2.2.3. The chromospheric and photospheric features of the disturbance source, a gas-dynamical disturbance

Figure 6a is the chromospheric Hβ brightness field within the rectangle of Fig. 1. The brightest areas marked with "1" and "2" in Fig. 6a correspond to the origins of the spray. Figure 6b displays the co-alignment of the brightest areas in Fig. 6a with the vortex-like red-shift area (Fig. 5). From Fig. 6b, we see that the spray origin, marked with "1", is "inlaid" is the red-shift thread spacing, where velocity is lower. It is well known that the spray is the projection of an upward ejecta against the solar disk (2.1.1), while the red-shift area shows the strong downward compression of the deep chromosphere (2.2.2). Thus, two kinds of movements with opposite directions, i.e. a downward compression and an upward ejection, occur in the disturbance source at the same time and propagate as a wave in the gas.

In addition, there were 6 patches of white light emission accompanying the flare. Figure 7a is the photospheric brightness field of the disturbance source region, Fig. 7b shows the co-alignment of the photospheric source region with the vortex-like red-shift area. The brightest areas, marked "C" and "D" in Fig. 7a, show where the white light flare (WLF) patches are located. These are very close to the vortex-like red-shift area (Fig. 7b). White light flares are suggested to result from the precipitation of hot electrons from the upper atmosphere (Fang 1997). Therefore, this coincidence of the WLF patches with the source of the Moreton wave further proves that the material within/near the disturbance source is compressed violently by the heating of the gas above the chromosphere. The strong compression itself indicates that a dynamical disturbance of the gas is at the origin of the Moreton wave.

2.2.4. Merging and emerging of the photospheric magnetic field in the disturbance source

The velocity field (in gray scale) and the magnetic field (in contours) map of the source region are overlaid in Fig. 8d. We see from this figure that the cross-section of the downward vortex-like plasma bubble is located in the magnetic region with positive polarity between two neutral lines

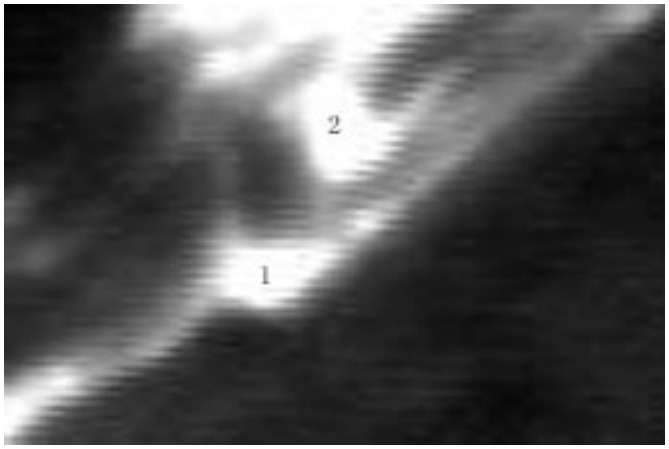

(a)

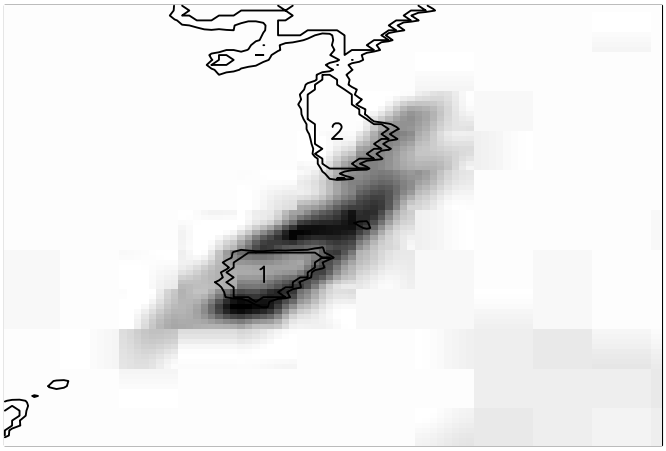

(b)

Fig. 6. a) A magnified map of the chromospheric Hβ intensity field within the rectangle in Fig. 1. **b)** The same as **a)** but in contours of brightness (the levels of the contours are 100% and 94% of peak-brightness), and the velocity field (gray-scaled, at 03:39:24 UT) of the disturbance source are co-aligned. The peak-contour (100%) marked with "1" is just "inlaid" between the darkest threads where the velocity is maximum.

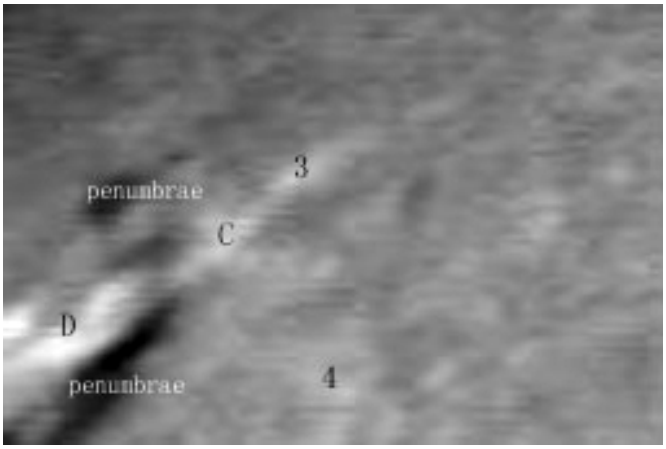

(a)

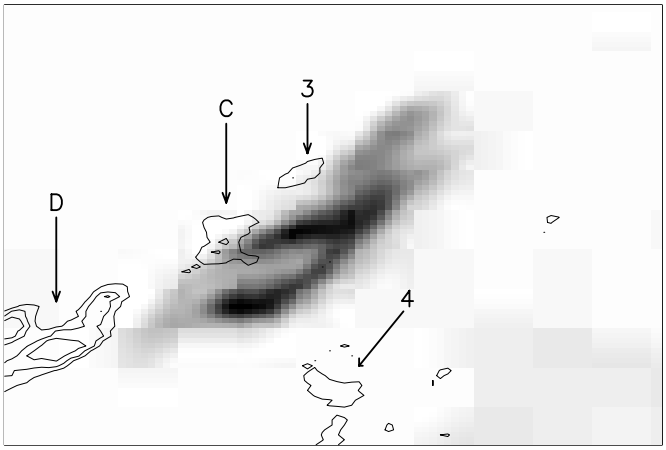

(b)

Fig. 7. a) The photosphere image (at 04:05:33 UT) of the disturbance source; the brighter places marked by "C" and "D" are coincident with the WLF patches "C" and "D". **b)** The photospheric image (in contours of brightness; the levels of the contours are 99.5% and 92.2% of peak-brightness) and velocity field (gray-scaled) of the disturbance source are co-aligned. The symbols "C" and "D" are the same as above, others marked by "3" and "4" are where the brightness is greater than 92.2% of peak-brightness.

(indicated as "N"), and is roughly in accordance with the magnetic field intensity contour of 110 Gauss. By examining the history of its magnetic field (Figs. 8a–c), it is obvious that the magnetic flux changes rapidly within the *N*-polarity region. At 00:28:59 UT (Fig. 8a), the 110 G-contour covers nearly half of the N-region, and contours inside the 110 G-contour show a field strength greater than 190 G in some places. However, later, at 01:37:24 UT, the field strength within the region was less than 110 G (Fig. 8b). Then, from 02:24:06 UT, small areas with a field strength of 110 G begin to emerge, and the total region is surrounded by the 110 G-contours until 04:05:55 UT (Fig. 8d). The N-polarity magnetic flux and the average strength within the source region during the period are estimated, and listed as Items 1, 2, 3, and 15 of Table 1. We can see from Table 1 that the magnetic flux of the region undergoes rapid variation during 3.6 hours (00:28:59–04:05:55 UT): it first decreases, then increases, suggesting the merging and emerging of the magnetic field.

3. Analysis of the observations, conclusion and discussion

Since the history of the Moreton wave phenomenon is quite complicated, and since the data concern the

Table 1. Summary of events relating to the flare and the Moreton wave.

Item	Time	Event recorded (relevant section)	Object concerned
1	00:28:59	Magnetic flux is 1.54×10^{20} Mx, averaged field strength is 79 G (Fig. 8a).	Disturbance source
2	01:37:24	Magnetic flux reduces to 0.68×10^{20} Mx, averaged field strength is 35 G (Fig. 8b).	Disturbance source
3	02:24:06	Magnetic flux begins to increase to 0.80×10^{20} Mx, averaged field strength is 44 G (Fig. 8c)	Disturbance source
4	03:37:25	The flare starts (1)	Flare
5	03:37:30	WLF patch-A occurs (2.2.3)	WLF patch
6	03:38:45	WLF patch-B and C occur (2.2.3)	WLF patch Border of the source
7	03:38:52	Spray origin starts to brighten (2.1.1)	Spray origin
8	03:38:58- 03:39:01	The front-tip of the spray moves 30 000 km (2.1.1)	Spray
9	03:39:00	WLF patch-D occurs (2.2.3)	WLF patch Border of the source
10	03:39:18.9- 03:39:24	The crests, troughs, and the disturbance source (red-shift area) are recorded by MFT on velocity field (2.1.3), and the red-shift velocity of the vortex-like bubble reaches its maximum (2.2.1)	Disturbance source Wavefronts
11	03:39:23- 03:39:25	Matter escaped from the spray trace (2.1.1)	Wavefronts
12	03:39:34- 03:44:04	Pictures of the wave propagation are taken by the Hα Patrol Telescope (full disk) (2.1.2)	Wavefronts
13	03:41:28- 03:41:54	The wavefronts are recorded by the SFT (FOV $5' \times 5'$) and by MFT (FOV $4' \times 6'$) on the monochromatic images (2.1.2)	Wavefronts
14	03:45:05	Velocity field map shows the relaxation of the vortex-like bubble (2.2.2)	Disturbance source
15	04:05:55	Magnetic flux increases continually to 2.58×10^{20} Mx, averaged field strength reaches to 124 G (Fig. 8d)	Disturbance source

chromospheric velocity field and the photospheric magnetic field, the observed characteristics of the events relevant to the flare and the Moreton wave are summarized in Table 1. An analysis of the observations and a discussion then are made, and finally, a conclusion is drawn.

Although identification of the disturbance source for the Moreton wave in 2.2.1 is only based on the geometric relationship between the red-shift area and concentric circles (wavefronts) around that area, additional events observed at the source support this identification. Since it is not accidental that so many important features, which are relevant to the wave and described in Sects. 2.2.2–2.2.4, are observed in the same region (the source), the identification in 2.2.1 is reasonable. All the observed features concerning the types of disturbances and acceleration of the Moreton wave; analysis and discussions are given as follows.

3.1. On the types of disturbances at the origin of Moreton waves

The observations presented in 2.2.4 indicate that the averaged magnetic field strength within the disturbance source varies rapidly before the propagation of the wave (see items 1–3 in Table 1) began. It decreases to less than half over about one hour, and then increases. The average (longitudinal) field strength B, increasing or decreasing, leads to magnetic pressure $\left(p = \frac{B^2}{8\pi}\right)$ increasing or decreasing. The magnetic pressure acts to push the plasma out from regions of higher magnetic pressure to regions where the magnetic pressure is lower. Variations in magnetic pressure cause the plasma around the source to move transversally: it would contract towards the source if the pressure within the source decreases, and would expand away from the source if the pressure increases. Thus, such a magnetohydrodynamic (MHD) effect may generate a propagating wave.

In addition, the fact that a prominent red-shift occurs within the source implies a strong downwards compression of the deep chromosphere, and may then be indirect evidence for explosive activity above the chromosphere and for release of mechanical energy, which might drive the Moreton wave. In fact, the observed WLF patches "C" and "D" fall within the border of the source, resulting from intense bombardment of the upper chromosphere by energetic electrons, since WLF is interpreted as electron-precipitation (Fang 1997; Hudson et al. 1992). Therefore,

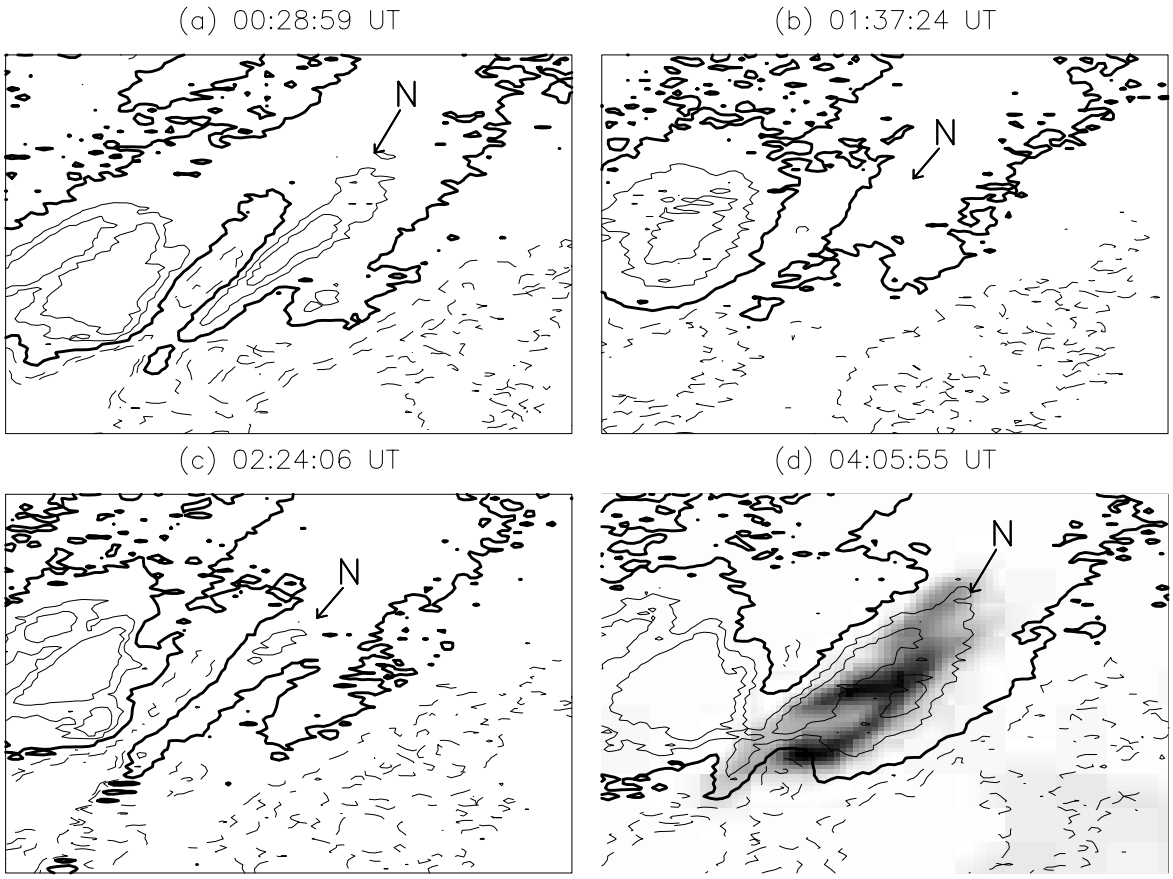

Fig. 8. a–c) Magnetic fields within the disturbance source. Thick-solid lines represent neutral lines of the field, while solid (or dashed) lines represent N (or S)-polarity. Contour levels are ±110 and ±190 Gauss. The letter "N" between the two neutral lines shows the location of the disturbance source. **d)** The magnetic field is co-aligned to the velocity field (gray-scaled, at 03:39:24 UT) of the disturbance source.

a dynamical disturbance of the gas could also drive the Moreton wave.

In order to generate a wave that propagates with a wavelength of 1.4×10^4 km and a primary velocity of about 2500 km s^{-1}, a period of 5.6 s is needed. Although the magnetic field observations presented did not show such a time scale, impulsive magnetic field variations might certainly occur, since a flare took place, and this impulsiveness cannot be detected by the usual magnetic field observations. Sampling of the magnetic field observations in the flare of AR6659 in June 4, 1992 occurred only at the times shown in Figs. 8a–d.

3.2. The acceleration of the Moreton wave

We known that the magnetic flux in the source continually increased during about 100 min from 02:24 UT (cf. items 3 and 15 of Table 1), as did the average longitudinal field strength B. In response to the magnetic field intensity increase by a factor of about 3 (from 44 G to 124 G), the relative magnetic pressure increased by factor of about 9. In general, magnetic pressure provides transverse forces to compress the plasma and balance the plasma pressure gradient (Priest 1982). However, the balance may be disrupted locally if the magnetic pressure increases faster than the plasma pressure gradient does, for instance, if the longitudinal field strength increases too rapidly. Thus, the difference between the magnetic pressure and the plasma pressure gradient can be the force that accelerates the Moreton wave, as well as the spray material.

3.3. The relationship of the Moreton wave with the spray

The Moreton wave accompanying the WLF of AR6659 on June 4, 1991 is observed to have a close relationship with a spray. Not only do the wave and the spray originate from a common source, but also the wavefronts have the same shape as the trace by which the spray ejected. Both the wavefronts and the spray show real mass motions and the wavefronts propagate toward the North Pole along the disk limb while the spray ejects upwards to enter the corona. They both are accelerated by the magnetic pressure to reach very high velocities: 4 000 km s^{-1} for the

wavefronts and 10 000 km s^{-1} for the spray. In spite of the similarities between the wave and the spray, they respectively present different kinds of motions. The wavefronts alternatively depress (lead towards a trough) and relax (to lead to a crest) in the chromosphere, while the spray ejects up into the corona. The former is visible for 280 s (03:39:24–03:44:04 UT, cf. items 10 and 12 of Table 1) on the disk, while the latter is visible only for 180 s (03:38:52–03:41:54 UT, cf. item 7 of Table 1 and Fig. 3c). Moreover, as indicated in Sect. 2.1.2, the spray was not the origin of the wave, since the wavefront sweep across the spray trace but did not come from the spray.

3.4. The "sweeping skirt hypothesis"

Uchida (1974) proposed that the Moreton wave is produced when the fast MHD shock wave propagates (refracted continually due to the gradient in the Alfven velocity) in the corona and the skirt of the wavefront swept across the chromosphere, i.e. the "sweeping skirt hypothesis". According to this hypothesis, the source driving the Moreton wave would be a flare shock wave, generated at the reconnection site somewhere in the corona. However, the observed results obtained from the Moreton wave in this article do not support the "sweeping skirt hypothesis". The reasons are the following:

(a) The estimated height of reconnection site is not consistent. The WLF produced by AR6659 on 1991 June 4 was observed with 6 white light patches (Sakurai et al. 1995) that could be interpreted as electron-precipitation. Assuming that the generation of the flare shock wave is simultaneous with the occurrence of the patches (actually, the shock wave should have occurred before), the shock wave presumably would have been generated at 03:37:30 UT (cf. item 5 of Table 1). Since the Moreton wave was observed at 03:39:24 UT (cf. item 10 of Table 1), the propagating time of the shock wave is 114 s. Considering that the shock wavefront propagated at the speed of 2500 km s^{-1} (Sakurai et al. 1995), the height of the reconnection site would be 285 Mm above the chromosphere. However, the estimate of a possible site of a current sheet, with reference to Yohkoh observations (Masuda et al. 1994; Sakao et al. 1992), shows that the above-deduced height of 285 Mm is not consistent. The Yohkoh observations have proved that the current sheet is above the soft X-ray flare loop (Masuda et al. 1994), and that impulsive hard X-ray double sources, which coincide with WLF patches, i.e. double feet of a loop, are of a non-thermal nature (Sakao et al. 1992). Based on the fact that two WLF patches "B" and "D" correspond to a pair of the feet of a single loop (Sakurai et al. 1995), the inferred height of the loop is only 2.86 Mm, provided that the loop takes a semi-circle form. Thus, a site of the current sheet is located somewhere above the loop, i.e. 1/100 of the height estimated from the "sweeping skirts hypothesis."

(b) Based on the above-mentioned (a), it is further considered that the shock wave front propagates from the corona to the chromosphere, i.e. the propagation was from the lower density region to the higher density region in the solar atmosphere. The velocity of the wavefront (e.g. the Alfven speed) should decrease. In other words, the velocity of 2500 km s^{-1} (Sakurai et al. 1995) was only a lower limit. If so, the height of the reconnection site " would still be higher than 285 Mm.

(c) The "sweeping skirt hypothesis" implies that the location of the disturbance source of the Moreton wave is in the corona level. However, the observations of the Moreton wave discussed in this article show that the disturbance source is located between the photosphere (where significant variations of the magnetic field, as well as WLF patches, were observed) and the upper-chromosphere (where red-shifted motions were observed).

3.5. Conclusions

(1) The source of disturbance for the Moreton wave occurs in the layers of the atmosphere between the photosphere and the upper-chromosphere. In the photosphere, the magnetic field merges or alternatively emerges; thus, the variation of the magnetic pressure is suggested to give rise to an MHD disturbance. In addition, the fact that two WLF patches "C" and "D" were observed very close to the source of the Moreton wave, and the fact that a prominent red-shift movement (Fig. 5) was observed in the source, prove that the material within/near the origin is compressed due to hot material expanding from the upper chromosphere. Thus, a gas-dynamic disturbance is produced. In addition, that the spray-upward ejection and the strong downward compression onto the deep chromosphere occur simultaneously in the disturbance source region is also able to cause the gas-dynamic disturbance.

(2) An MHD disturbance is coupled with a gas-dynamic disturbance to generate the Moreton wave observed in the WLF produced by AR6659 at June 4, 1991.

(3) Although the onset (03:38:52 UT, cf. item 7 of Table 1) of the spray is a little earlier than the time when the wavefront begins to be visible (03:39:24 UT, cf. item 10 of Table 1), the spray cannot be identified as the origin of the wavefronts, because the wavefronts are traveling across the spray trace (Figs. 2g,h), rather than originating from it.

Acknowledgements. The author thanks the Japanese Society for the Promotion of Science (JSPS) for an invitation to visit the NAOJ and the University of Tokyo. Also the author would like to express her deep thanks to Prof. Takashi Sakurai, who has corrected some points and proposed Table 1. This work is

supported by the Scientific Application Foundation of Yunnan Province, item No. 1999A0088M.

References

Dodson, H. W., & Hedeman, E. R. 1968, Solar Phys., 4, 229,
Fang, Cheng 1997, Progress in Astronomy, 15, 27,
Hudson, H. S., Acton, L. W., Hirayama, T., & Uchida, Y. 1992, PASJ, 44, L77
Masuda, S., Kosugi, T., Hara, H., Tsuneta, S., & Ogawara, Y. 1994, Nature, 371, 495
Moreton, G. E. 1964, ApJ, 69, 145,
Moses, D., Clette, F., Delaboudinière, J.-P., et al. 1997, Solar Phys., 175, 571
Priest, E. 1982, Solar Magneto-hydrodynamics (Dordrecht: Reidel)
Sakao, T., Kosugi, T., Masuda, S., et al. 1992, Publs Astr. Soc. Japan, 44, L83,
Sakurai, T., Irie, M., Miyashita, M., Yamaguchi, K., & Shiomi, Y. 1995, Proc. Of the Second SOLTIP Symposium, 33
Smith, S. F., & Harvey, K. 1971, Physics of the Solar Corona, in ed. C. J. Macris, 156
Uchida, Y. 1974, in Coronal Disturbances, Proc. IAU Symp., 57, ed. G. A. Newkirk Jr. (Reidel, Dordrecht), 383
Wild, J. P. 1968 in Plasma Instabilities In Astrophysics, ed. D. G. Wentzel, & D. A. Tidman, 119, 1968
Zhang Heng, Wu Mingchan, & Li Yongsheng 1996, Acta Astrophysics Sinica, 16, No. 4, 408,
Zhang Hongqi, Ai Guoxiang, Yan Xu, Li Wei, & Liu Yang 1994, ApJ, 423, 828
Zirin, H., & Russo Lackner, D. 1969, Solar Phys., 6, 86